frontiers | Frontiers in Marine Science

TYPE Original Research
PUBLISHED 22 January 2024
DOI 10.3389/fmars.2024.1294608

Check for updates

OPEN ACCESS

EDITED BY
Paulo Sergio Salomon,
Federal University of Rio de Janeiro, Brazil

REVIEWED BY
Hyun Je Park,
Gangneung-Wonju National University, Republic of Korea
Patrick Rafter,
University of California, Irvine, United States

*CORRESPONDENCE
Chisato Yoshikawa
yoshikawac@jamstec.go.jp

RECEIVED 15 September 2023
ACCEPTED 03 January 2024
PUBLISHED 22 January 2024

CITATION
Yoshikawa C, Shigemitsu M, Yamamoto A, Oka A and Ohkouchi N (2024) A nitrogen isoscape of phytoplankton in the western North Pacific created with a marine nitrogen isotope model.
Front. Mar. Sci. 11:1294608.
doi: 10.3389/fmars.2024.1294608

COPYRIGHT
© 2024 Yoshikawa, Shigemitsu, Yamamoto, Oka and Ohkouchi. This is an open-access article distributed under the terms of the Creative Commons Attribution License (CC BY). The use, distribution or reproduction in other forums is permitted, provided the original author(s) and the copyright owner(s) are credited and that the original publication in this journal is cited, in accordance with accepted academic practice. No use, distribution or reproduction is permitted which does not comply with these terms.

A nitrogen isoscape of phytoplankton in the western North Pacific created with a marine nitrogen isotope model

Chisato Yoshikawa[1]*, Masahito Shigemitsu[2], Akitomo Yamamoto[2], Akira Oka[3] and Naohiko Ohkouchi[1]

[1]Biogeochemistry Research Center, Research Institute for Marine Resources Utilization, Japan Agency of Marine-Earth Science and Technology (JAMSTEC), Yokosuka, Japan, [2]Research Institute for Global Change (RIGC), JAMSTEC, Yokosuka, Japan, [3]Atmosphere and Ocean Research Institute, The University of Tokyo, Kashiwa, Chiba, Japan

The nitrogen isotopic composition ($\delta^{15}N$) of phytoplankton varies substantially in the ocean reflecting biogeochemical processes such as N_2 fixation, denitrification, and nitrate assimilation by phytoplankton. The $\delta^{15}N$ values of zooplankton or fish inherit the values of the phytoplankton on which they feed. Combining $\delta^{15}N$ values of marine organisms with a map of $\delta^{15}N$ values (i.e., a nitrogen isoscape) of phytoplankton can reveal the habitat of marine organisms. Remarkable progress has been made in reconstructing time-series of $\delta^{15}N$ values of migratory fish from various tissues, such as otoliths, fish scales, vertebrae, and eye lenses. However, there are no accurate nitrogen isoscapes of phytoplankton due to observational heterogeneity, preventing improvement in the accuracy of estimating migratory routes using the fish $\delta^{15}N$ values. Here we present a nitrogen isoscape of phytoplankton in the western North Pacific created with a nitrogen isotope model. The simulated phytoplankton is relatively depleted in ^{15}N at the subtropical site (annual average $\delta^{15}N$ value of phytoplankton of 0.6‰), where N_2 fixation occurs, and at the subarctic site (2.1‰), where nitrate assimilation by phytoplankton is low due to iron limitation. The simulated phytoplankton is enriched in ^{15}N at the Kuroshio–Oyashio transition site (3.9‰), where nitrate utilization is high, and in the region around the Bering Strait site (6.7‰), where partial nitrification and benthic denitrification occur. The simulated $\delta^{15}N$ distributions of nitrate, phytoplankton, and particulate organic nitrogen are consistent with $\delta^{15}N$ observations in the western North Pacific. The seamless nitrogen isoscapes created in this study can be used to improve our understanding of the habitat of marine organisms or fish migration in the western North Pacific.

KEYWORDS

isoscape, nitrogen isotopes, marine nitrogen cycle, nitrogen isotope model, western North Pacific

1 Introduction

Identifying the migration routes of marine animals is crucial for sustainable fisheries management and biodiversity conservation. Many methods, such as catch per unit effort with location (e.g., Thorson et al., 2016), dart tag/capture studies (e.g., Hanselman et al., 2015), and bio-logging (e.g., Hays et al., 2016), are used to study the migration routes. Although tracking technologies have advanced greatly, the migration routes over the entire life cycle of marine animals, including the spawning sites or the larval and juvenile habitats, are often unknown due to body size limitations (Lowerre-Barbieri et al., 2019). Chemical signatures in otoliths and other body parts have become a promising tool for tracing these migration routes (Tzadik et al., 2017).

The isotopic composition of animal tissues and local environments can be used as a natural tag to track an animal's movements through isotopically distinct habitats, called iso-logging (Matsubayashi et al., 2022). Nitrogen isotope ($\delta^{15}N$) analysis of incremental growth tissues, such as eye lenses and vertebral bones, has proven promising for reconstructing migration routes and feeding environments over the animal's life (Matsubayashi et al., 2017; Matsubayashi et al., 2020; Vecchio and Peebles, 2020; Harada et al., 2022). It is essential to understand the spatial variations in $\delta^{15}N$ values (nitrogen isoscapes) across the habitat for using the $\delta^{15}N$ values for iso-logging of marine animals. However, seamless nitrogen isoscapes are generally difficult to obtain through field sampling (McMahon et al., 2013; Matsubayashi et al., 2020; Fripiat et al., 2021) because there are wide spatial and temporal variations in $\delta^{15}N$ values.

The variations in $\delta^{15}N$ values reflect biogeochemical processes. When phytoplankton assimilates nitrate, nitrogen isotopes are fractionated (Wada and Hattori, 1978; Montoya and McCarthy, 1995). The $\delta^{15}N$ value of nitrate ($\delta^{15}N_{Nitrate}$) increases as nitrate consumption increases due to an isotopic effect ranging from 5‰ to 8‰ during nitrate assimilation by phytoplankton (Granger et al., 2010). When denitrification occurs in the water column, the $\delta^{15}N_{Nitrate}$ value increases dramatically due to a strong isotopic effect of ~15‰ (Granger et al., 2008). N_2-fixation produces fixed nitrogen with a $\delta^{15}N$ value of ~0‰, because nitrogen fixers take up N_2 with little isotopic effect (Minagawa and Wada, 1986). This fixed nitrogen with a low $\delta^{15}N$ value is eventually converted into nitrate with a low $\delta^{15}N$ value through the degradation of nitrogenous organic compounds via remineralization and subsequent nitrification. The spatial patterns of $\delta^{15}N_{Nitrate}$ values in the euphotic zone are conserved in phytoplankton and are subsequently transferred to organisms with higher trophic positions (zooplankton and fish) with ^{15}N enrichment of ~3‰ per trophic position (Minagawa and Wada, 1984).

In this study, we developed a marine nitrogen isotope model that includes biogeochemical processes, and we generated a seamless nitrogen isoscape of phytoplankton as the base of the food web ($\delta^{15}N_{Base}$) in the western North Pacific for iso-logging studies. The western North Pacific, the focus of this article, is one of the most biologically diverse and productive fishery regions (FAO, 2022). Identifying fish movements in the western North Pacific is commercially important for pelagic fish in countries in the Asia–Pacific region.

2 Model description

2.1 Nitrogen isotope model

The marine nitrogen isotope model used in this study has seven compartments: phytoplankton (PHY), diazotrophs (DIA), zooplankton (ZOO), particulate organic nitrogen (PON), dissolved organic nitrogen (DON), nitrate (NO_3^-), ammonium (NH_4^+), and dinitrogen (N_2) (Figure 1). The prognostic variables are the N and ^{15}N concentrations of these compartments, except N_2. The concentration of N_2 is set to always be sufficient for DIA and the $\delta^{15}N$ value is set as 0‰. The equations for the N and ^{15}N cycles are essentially the same as those used by previous modeling studies in the western North Pacific (Yoshikawa et al., 2005; Yoshikawa et al., 2016; Yoshikawa et al., 2022). The parameters and isotopic fractionation factors used here are shown in Tables 1, 2, respectively. The N_2 fixation and denitrification schemes are introduced in this study.

2.2 N_2 fixation and denitrification

The N_2 fixation scheme is a modified version of the model developed by Hood et al. (2001) (see also Coles et al., 2004; Hood et al., 2004; Coles and Hood, 2007; Yoshikawa et al., 2013). The prognostic variable of DIA is calculated as a function of time, t, and each grid using the following governing equations.

$$d[\mathrm{DIA}]/dt = (\mathrm{Growth}_{\mathrm{DIA}}) - (\mathrm{Mortality}_{\mathrm{DIA}}) - (\mathrm{Grazing}_{\mathrm{DIA}}) - (\mathrm{Extracellular\ Excretion}_{\mathrm{DIA}}) \quad (1)$$

Growth $_{\mathrm{DIA}}$ in Equation 1 is modeled by:

$$(\mathrm{Growth}_{\mathrm{DIA}}) = \mu_T\left(1 - e^{-I/I_T}\right)(\min([\mathrm{DIP}]/([\mathrm{DIP}] + K_{PT}), [\mathrm{Fe}]/([\mathrm{Fe}] + K_{FeT}))[\mathrm{DIA}] \quad (2)$$

which describes light-, dissolved inorganic phosphorous (DIP)-, and Fe-dependent variations in diazotroph growth. In Equation 2, μ_T is the maximum growth rate. Variable I is the irradiance, and I_T is the light saturation parameter. In addition, K_{PT} and K_{FeT} are half-saturation constants for diazotroph DIP and Fe uptake. Diazotrophs fix N_2 with 0‰ and no isotopic fractionation (ϵ_9). The diazotroph nitrate uptake is modeled by:

$$(\mathrm{Nitrate\ assimilation}_{\mathrm{DIA}}) = \mu_T\left(1 - e^{-I/I_T}\right)(\min([NO_3^-]/[NO_3^-] + K_{NT}), [\mathrm{DIP}]/([\mathrm{DIP}] + K_{PT}), [\mathrm{Fe}]/([\mathrm{Fe}] + K_{FeT}))[\mathrm{DIA}] \quad (3)$$

where K_{NT} is the half-saturation constant for nitrate. Although diazotrophs take up nitrate, their growth rate is not limited by nitrate availability. Thus, when nitrate concentrations are very low, diazotroph growth is supported almost entirely by N_2 fixation.

10.3389/fmars.2024.1294608

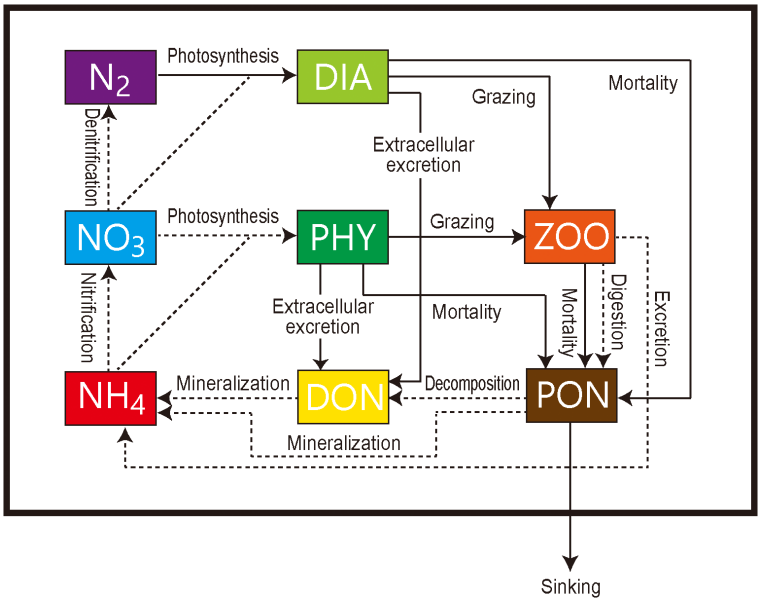

FIGURE 1
Schematic of the marine ecosystem isotope model. NO_3^-, nitrate concentration; NH_4^+, ammonium; N_2, dinitrogen; PHY, phytoplankton; DIA, diazotrophs; ZOO, zooplankton; PON, particulate organic nitrogen; DON, dissolved organic nitrogen. Dashed and solid arrows indicate nitrogen flows with and without isotopic fractionation, respectively.

TABLE 1 Biological parameters in the nitrogen isotope model.

Symbol	Parameter	Value		Citation
V_{max}	Phytoplankton maximum photosynthetic rate at 0 °C	0.25	/day	Yoshikawa et al. (2022)
K_{NO3}	Phytoplankton half saturation constant for nitrate	2.0	μmolN/L	Yoshikawa et al. (2022)
K_{NH4}	Phytoplankton half saturation constant for ammonium	0.2	μmolN/L	Yoshikawa et al. (2022)
ψ	Phytoplankton ammonium inhibition coefficient	1.5	L/μmolN	Yoshikawa et al. (2022)
k	Phytoplankton temperature coefficient for photosynthesis	0.0693	/°C	Yoshikawa et al. (2022)
I_{opt}	Phytoplankton optimum light intensity	100.0	W/m^2	Yoshikawa et al. (2022)
M_{p0}	Phytoplankton mortality rate at 0 °C	0.04375	L/μmolN/day	Yoshikawa et al. (2022)
k_{Mp}	Phytoplankton temperature coefficient for mortality	0.0693	/°C	Yoshikawa et al. (2022)
μ_T	Diazotroph maximum growth rate	0.23	/day	Yoshikawa et al. (2013)
K_{NT}	Diazotroph half saturation constant for nitrate	0.5	μmolN/L	Yoshikawa et al. (2013)
K_{PT}	Diazotroph half saturation constant for phosphate	0.0077	μmolN/L	Yoshikawa et al. (2013)
K_{FeT}	Diazotroph half saturation constant for iron	0.0001	μmolN/L	Yoshikawa et al. (2013)
I_T	Diazotroph light saturation	70.0	W/m^2	Yoshikawa et al. (2013)
S_T	Diazotroph mortality rate	0.005	/day	Yoshikawa et al. (2013)
γ	Ratio of extracellular excretion to photosynthesis	0.135	(nodim.)	Yoshikawa et al. (2022)
G_{Rmax}	Zooplankton maximum grazing rate of phytoplankton at 0 °C	0.3	/day	Yoshikawa et al. (2022)
G_{RmaxT}	Zooplankton maximum grazing rate of diazotrophs at 0 °C	0.1	/day	*
k_G	Zooplankton temperature coefficient for grazing	0.0693	/°C	Yoshikawa et al. (2022)
λ	Zooplankton ivlev constant	1.4	L/μmolN	Yoshikawa et al. (2022)
P^*_Z	Zooplankton threshold value for grazing	0.04	μmolN/L	Yoshikawa et al. (2022)

(Continued)

TABLE 1 Continued

Symbol	Parameter	Value		Citation
α	Zooplankton assimilation efficiency	0.7	(nodim.)	Yoshikawa et al. (2022)
β	Zooplankton growth efficiency	0.3	(nodim.)	Yoshikawa et al. (2022)
M_{z0}	Zooplankton mortality rate at 0 °C	0.0585	L/μmolN/day	Yoshikawa et al. (2022)
k_{Mz}	Zooplankton temperature coefficient for mortality	0.0693	/°C	Yoshikawa et al. (2022)
α_1	Light dissipation coefficient of sea water	0.04	/m	Yoshikawa et al. (2022)
α_2	Self shading coefficient	0.054	L/μmolN/m	Yoshikawa et al. (2022)
α_3	Self shading coefficient	0.6667	(nodim.)	Yoshikawa et al. (2022)
α_4	Self shading coefficient	0.0088	L/μmolN/m	Yoshikawa et al. (2022)
R_{chla}	Chlorophyll to nitrogen ratio	1.59	(nodim.)	Yoshikawa et al. (2022)
S_{PON}	PON sinking velocity at the surface layer	7.00	m/day	Schmittner et al. (2008)
m_w	Increase of sinking speed with depth	0.04	/day	Schmittner et al. (2008)
N_{Nit0}	Nitrification rate at 0 °C	0.6	/day	Yoshikawa et al. (2022)
k_{Nit}	Temperature coefficient for nitrification	0.0693	/°C	Yoshikawa et al. (2022)
I_1	Light inhibition coefficient for nitrification	0.0364	W/m^2	Yoshikawa et al. (2022)
I_2	Light inhibition coefficient for nitrification	0.074	W/m^2	Yoshikawa et al. (2022)
V_{PA0}	Remineralization rate of PON to ammonium at 0 °C	0.1	/day	Yoshikawa et al. (2022)
k_{PA}	Temperature coefficient for PON remineralization to ammonium	0.0693	/°C	Yoshikawa et al. (2022)
V_{PD0}	Decomposition rate of PON to DON at 0 °C	0.1	/day	Yoshikawa et al. (2022)
k_{PD}	Temperature coefficient for POM decomposition to DON	0.0693	/°C	Yoshikawa et al. (2022)
V_{DA0}	Remineralization rate of DON to ammonium at 0 °C	0.01	/day	**
k_{DA}	Temperature coefficient for DON remineralization to ammonium	0.0693	/°C	Yoshikawa et al. (2022)
$R_{O:N}$	Atomic ratio of O to N	8.652	(nodim.)	Hajima et al. (2020)
D_{min}	Nitrate threshold for water column denitrification	50.0	μmolN/L	***
α_{BD}	Benthic denitrification coefficient	0.3	(nodim.)	***

* The G_{Rmax} of diazotrophs is reduced from 0.3 to 0.1 /day to reproduce the observed abundance of diazotrophs compiled by Yoshikawa et al. (2013).
** The V_{DA0} is reduced from 0.1 /day (Yoshikawa et al., 2022) to 0.01 /day to reproduce the surface DON concentrations observed by Letscher et al. (2013).
*** The D_{min} and α_{BD} are tuned to set the global fluxes of water column denitrification and benthic denitrification in the model to the previous estimates (see the main text).

Mortality $_{DIA}$ in Equation 1 is modeled using:

$$(\text{Mortality}_{\text{DIA}}) = S_T[\text{DIA}] \quad (4)$$

where S_T is the mortality rate of DIA.

Grazing $_{DIA}$ in Equation 1 is modeled using:

$$(\text{Grazing}_{\text{DIA}}) = G_{RmaxT}(\max(0, 1 - \exp(\lambda(P_\star z - [\text{DIA}])))\exp(K_G T)[\text{ZOO}] \quad (5)$$

where G_{RmaxT}, λ, and P^*z are the zooplankton maximum grazing rate for DIA, zooplankton Ivlev constant, and zooplankton threshold value for grazing, respectively. Variable T is the temperature, and K_G is the zooplankton temperature coefficient for mortality.

Extracellular Excretion $_{DIA}$ in Equation 1 is modeled by:

$$(\text{Extracellular Excretion}_{\text{DIA}}) = \gamma(\text{Growth}_{\text{DIA}}) \quad (6)$$

where γ is the ratio of extracellular excretion of DIA to growth.

The water-column denitrification scheme is essentially the same as that reported by Schmittner et al. (2008). Oxygen consumption in suboxic waters (<3 μM) is inhibited and replaced by the oxygen-equivalent oxidation of nitrate:

$$r_{NO3} = 0.5(1 - \tanh([O_2] - 3.0)) \quad (7)$$

Denitrification consumes nitrate at a rate of 80% of the oxygen equivalent rate, according to:

$$(\text{Denitrification}) = ((\text{Decomposition}) + (\text{Excretion}) + (\text{Remineralization}) - (\text{Growth}_{\text{PHY}}) - (\text{Growth}_{\text{DIA}}))(-0.8D_{flag}R_{O:N}r_{NO3}) \quad (8)$$

where $R_{O:N}$ is the ratio of O to N. D_{flag} limits the rate of water column N-loss at a given nitrate threshold of D_{min}:

$$D_{flag} = 0.5 + \text{sign}(0.5, [NO_3^-] - D_{min}) \quad (9)$$

TABLE 2 Isotope fractionation factors in the nitrogen isotope model.

Process	ϵ (‰)	Citation
NO_3^- assimilation by phytoplankton or diazotroph	$\epsilon_1 = 5$	Yoshikawa et al. (2005)
NH_4^+ assimilation by phytoplankton	$\epsilon_2 = 0$	*
Excretion by zooplankton	$\epsilon_3 = 5$	Yoshikawa et al. (2022)
Egestion by zooplankton	$\epsilon_4 = 2$	Yoshikawa et al. (2022)
Nitrification	$\epsilon_5 = 14$	Yoshikawa et al. (2022)
Remineralization from PON to DON	$\epsilon_6 = 1$	Yoshikawa et al. (2022)
Remineralization from DON to NH_4^+	$\epsilon_7 = 1$	Yoshikawa et al. (2022)
Remineralization from PON to NH_4^+	$\epsilon_8 = 1$	Yoshikawa et al. (2022)
N_2 fixation by diazotroph	$\epsilon_9 = 0$	**
Water column denitrification	$\epsilon_{10} = 25$	**
Benthic denitrification	$\epsilon_{11} = 1$	**

* There are no previous estimates at ammonium concentrations < 4 μM. However, Liu et al. (2013) implied that the isotope effect in the surface water of the open ocean (<1 μM) may be much smaller than previous estimates of 5‰–18‰. Therefore, the isotope fractionation factor (ϵ_2) is reduced from 10 ‰ (Yoshikawa et al., 2022) to 0‰ in this study.
** The isotope fractionation factors (ϵ_9, ϵ_{10}, and ϵ_{11}) are introduced in this study and are set within field estimates (0‰–2‰, 22‰–30‰, and 0‰–4‰, respectively) compiled by Somes et al. (2010).

The isotopic fractionation factor for water-column denitrification (ϵ_{10}) is set to 25‰.

The benthic denitrification scheme is essentially the same as that reported by Shigemitsu et al. (2016). The benthic denitrification flux is parameterized based on the organic carbon flux to the seafloor (F_{POC_bot}) and bottom water O_2 and NO_3^- concentrations ($[O_2]_{bottom}$ and $[NO_3^-]_{bottom}$) as:

$$F_{BD} = \alpha_{BD} \cdot F_{POC\_bot} \left(0.06 + 0.19 \times 0.99^{[O_2]_{bottom} - [NO_3^-]_{bottom}}\right) \quad (10)$$

where α_{BD} is tuned to set the globally integrated rates of benthic denitrification in the model to the rates within the range of previous estimates (80–140 Tg N yr^{-1}; Bianchi et al., 2012; Bohlen et al., 2012; DeVries et al., 2013; Somes et al., 2013; Shigemitsu et al., 2016; Somes et al., 2017). The isotopic fractionation factor for benthic denitrification (ϵ_{11}) is set to 1‰.

2.3 Offline biogeochemical model

The nitrogen isotope model was incorporated into the ocean general circulation model (COCO) with an offline method (Oka et al., 2008; Shigemitsu et al., 2016). The model has 256 × 198 grid points in the horizontal direction and 44 vertical layers. The horizontal resolution is about 1°, and the vertical spacing varies from 5 m at the top to 250 m at the bottom. The concentration of biogeochemical tracers is calculated by the following tracer equation:

$$\frac{\partial C}{\partial t} = -\nabla \cdot (vC) + K_H \nabla_H^2 C + \frac{\partial}{\partial z}\left(K_V \frac{\partial C}{\partial z}\right) + S_C \quad (11)$$

where C is the tracer concentration, v is the velocity, K_H and K_V are the horizontal and vertical diffusivity, and S_C is the source/sink term for the tracer due to biogeochemical processes. The model was driven by climatological monthly mean physical fields (horizontal ocean velocities, vertical diffusivity, temperature, salinity, sea surface height, sea surface wind speed, sea ice fraction, and sea surface solar radiation) obtained from the outputs of a pre-industrial control simulation performed with an Earth system model (MIROC-ESM) (Watanabe et al., 2011) as in Shigemitsu et al. (2017). The climatological monthly mean concentration of dissolved iron was obtained from the output of a pre-industrial control simulation performed with an ocean biogeochemical model including an iron cycle (Yamamoto et al., 2019). In order to rapidly reach steady state, the initial conditions were set to values that have already reached steady state and were within the range of observations. The initial conditions of the nitrogen, phosphate, and oxygen concentrations were obtained from the outputs of a pre-industrial control simulation with MIROC-ESM (Watanabe et al., 2011). The initial conditions of $\delta^{15}N$ of PHY, DIA, ZOO, PON, DON, NO_3^-, and NH_4^+ were set to constant values of 3‰, 0‰, 6‰, 6‰, 6‰, 5‰, and 6‰, respectively. The results of the simulations presented here are shown after 3000 years of time integration.

3 Results

3.1 Horizontal distributions of nitrate and chlorophyll *a* concentrations

The simulated distributions of annual mean nitrate and chlorophyll *a* concentrations in the surface layer are generally consistent with the climatological annual mean concentrations of the World Ocean Atlas 2018 (Garcia et al., 2019) and the SeaWiFS satellite data (O'Reilly et al., 1998), respectively (Figure 2). The model represents the high nitrate concentrations exceeding 5 μM observed in the subarctic region and the low concentrations below 2 μM observed in the subtropical region (Figures 2A, C). Because of the nitrate availability, the simulated chlorophyll *a* concentrations are also high in the subarctic region and low in the subtropical region (Figures 2B, D). The root-mean-square error (RMSE), which is an estimate of the absolute magnitude of the difference between the observed and modeled values, is relatively high in the northwestern North Pacific for both nitrate and chlorophyll *a* concentrations (Figures 2E, F). This is because of the lack of terrestrial inputs of nitrogenous nutrients in the model and its coarse resolution. The extremely high RMSE in the coastal region for the chlorophyll *a* concentration may also be attributed to the

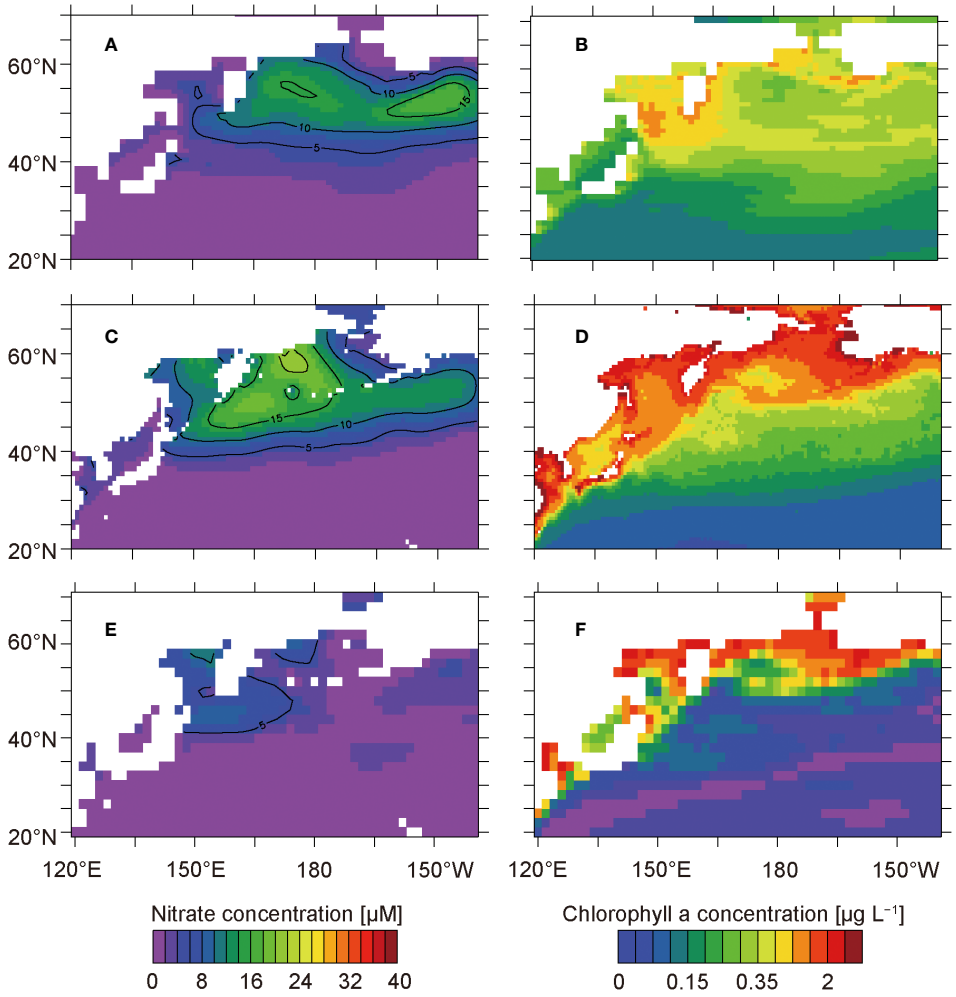

FIGURE 2
Concentrations of annual mean nitrate and chlorophyll *a* at the surface from the model simulations **(A, B)** and observations **(C, D)**. Panels **(C, D)** show the climatological annual mean nitrate concentrations in the surface waters of the World Ocean Atlas 2018 (Garcia et al., 2019) and the climatological annual mean chlorophyll *a* concentrations based on the SeaWiFS satellite data from 1997 to 2006 (O'Reilly et al., 1998), respectively. Panels **(E, F)** show the root-mean-square error of the model simulations of nitrate and chlorophyll *a* concentrations, respectively.

difficulty of satellite-based chlorophyll *a* estimation caused by terrestrial inputs of colored dissolved organic matter or suspended particles.

3.2 Horizontal distributions of $\delta^{15}N_{Nitrate}$, $\delta^{15}N_{Phytoplankton}$, and $\delta^{15}N_{PON}$ values

The simulated annual mean $\delta^{15}N$ values of nitrate in the surface layer and phytoplankton and PON in the euphotic layers have similar high–low distributions, except in the Bering Strait (Figure 3). The model represents the ^{15}N depletion observed in the subtropical and subarctic regions and the ^{15}N enrichment observed in the Oyashio–Kuroshio transition region. The model also represents the overall observed ^{15}N enrichment of nitrate and ^{15}N depletion of phytoplankton.

The simulated values are not precisely consistent with the observed values shown in Figure 3 for the following reasons. The simulated $\delta^{15}N_{Nitrate}$ values (Figure 3A) are annual mean surface values, whereas the observed values (Figure 3D) are the shallowest data that were measured in a single expedition compiled by Rafter et al. (2019) and Fripiat et al. (2021). The simulated $\delta^{15}N_{Phytplankton}$ values (Figure 3B) are the weighted averages of the euphotic layer throughout the year, whereas the observed values (Figure 3E) are the $\delta^{15}N_{Base}$ values estimated from the $\delta^{15}N$ measurements of bulk nitrogen and amino acids of zooplankton obtained from various depths and seasons (Matsubayashi et al., 2022). The simulated $\delta^{15}N_{PON}$ values (Figure 3C) are the weighted averages of the euphotic layer throughout the year, whereas the observed values (Figure 3F) are the $\delta^{15}N_{Bulk}$ values of surface sediments obtained from various depths and redox conditions compiled by NICOPP (Tesdal et al., 2013), which could be affected by digenesis.

For the discussion, we selected four representative sites in the western subtropical North Pacific (ST: 145°E, 22°N), the Kuroshio–Oyashio transition zone (TR: 155°E, 44°N), the western subarctic North Pacific (SA: 170°E, 55°N), and the Bering Strait region (BS: 190°E, 60°N) (Figure 3). The simulated $\delta^{15}N_{Nitrate}$ values in the surface layer are 1.1‰ at ST, 7.3‰ at TR, 6.8‰ at SA, and 6.6‰ at

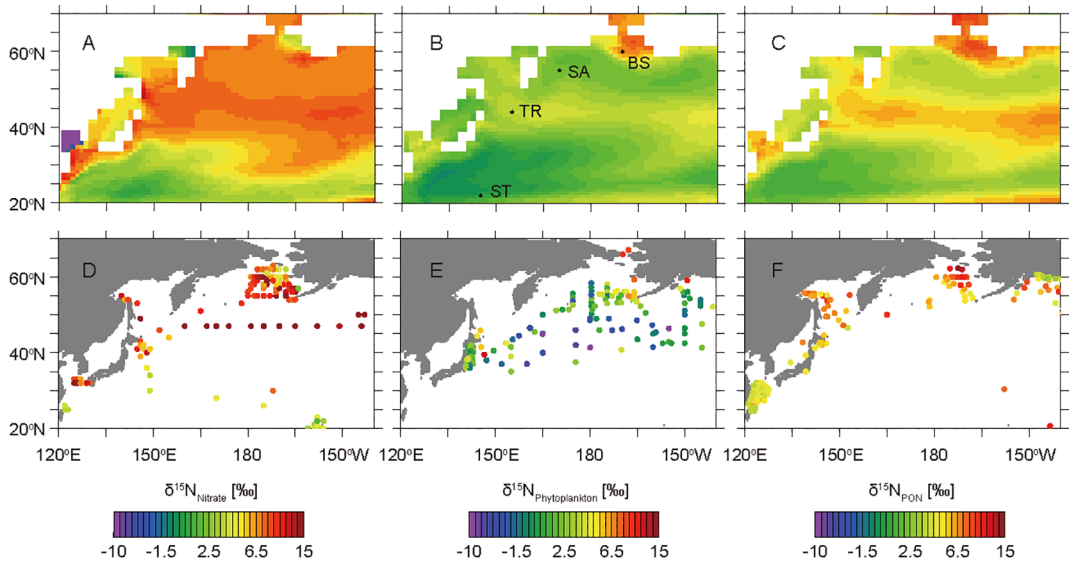

FIGURE 3
Horizontal $\delta^{15}N$ distributions of annual mean nitrate, phytoplankton, and PON from the model simulations **(A–C)** and observations **(D–F)**. Panels **(A-C)** show the $\delta^{15}N_{Nitrate}$ values at the surface layer, the weighted average of $\delta^{15}N_{Phytoplankton}$ values in the layers at 0–200 m, and the weighted average of $\delta^{15}N_{PON}$ values in the layers at 0–200 m, respectively. Panels **(D-F)** show the shallowest $\delta^{15}N_{Nitrate}$ values compiled by Rafter et al. (2019) and Fripiat et al. (2021), the $\delta^{15}N_{Base}$ values estimated from the $\delta^{15}N$ measurements of bulk nitrogen and amino acids of zooplankton (Matsubayashi et al., 2022), and the $\delta^{15}N$ values of surface sediments compiled by NICOPP (Tesdal et al., 2013), respectively. Locations of the western subtropical North Pacific site (ST: 145°E, 22°N), the Kuroshio–Oyashio transition zone site (TR: 155°E, 44°N), the western subarctic North Pacific site (SA: 170°E, 55°N), and the Bering Strait region site (BS: 190°E, 60°N) selected for this study are shown.

BS (Figure 3A). In the uppermost 200 m layers, the simulated weighted averages of $\delta^{15}N_{Phytoplankton}$ are 0.6‰ at ST, 3.9‰ at TR, 2.1‰ at SA, and 6.7‰ at BS (Figure 3B), whereas those of $\delta^{15}N_{PON}$ are 1.8‰ at ST, 5.9‰ at TR, 3.7‰ at SA, and 7.3‰ at BS (Figure 3C).

3.3 Seasonal cycles of nitrate, ammonium and phytoplankton concentrations

At ST, the simulated nitrate in the surface layer is depleted to<0.2 μM throughout the year and shows a slight increase from February to March (Figure 4A). The simulated ammonium accumulates slightly up to 0.02 μM in the layers at depths of 40–80 m from April to November (Figure 4B). The simulated phytoplankton concentration is low (<0.1 μM), equivalent to 0.2 μg Chl L^{-1}, throughout the year and has a small bloom in April (Figure 4C).

At TR, the simulated nitrate in the surface layer reaches a maximum concentration of 8.5 μM in March and is depleted to 0.3 μM in August (Figure 4D). Then, until March, the nitrate concentration increases as the surface mixed layer deepens. The simulated ammonium accumulates to >0.3 μM in the layers at 30–60 m from May to November, and the maximum concentration is 0.9 μM at a depth of 40 m in August (Figure 4E). The simulated phytoplankton has high concentrations of >0.1 μM throughout the year and has a bloom in June (Figure 4F).

At SA, the simulated nitrate in the surface layer reaches a maximum concentration of 17.0 μM in April and decreases to 10.4 μM in August (Figure 4G). The simulated ammonium accumulates to >0.3 μM in the layers at 30–60 m from July to October, and the maximum concentration is 0.6 μM at a depth of 40 m in August (Figure 4H). The simulated phytoplankton has high concentrations of >0.1 μM from April to October and has a bloom in June (Figure 4I).

At BS, the simulated nitrate in the surface layer reaches a maximum concentration of 3.8 μM in March and decreases to 1.9 μM in September (Figure 4J). The nitrate concentration in the bottom layer is<1.0 μM in July and August. The simulated ammonium accumulates to >2.0 μM in the bottom layer in July and August (Figure 4K), and then spreads to the upper layers as the surface mixed layer deepens from September to December. Then, until April, the ammonium concentration drops to 0.3 μM. The simulated phytoplankton has a high concentration of >0.1 μM from February to October and has blooms in June and August (Figure 4L).

3.4 Seasonal cycles of $\delta^{15}N$ values of nitrate, ammonium and phytoplankton

At ST, the simulated $\delta^{15}N_{Nitrate}$ value in the surface layer is 0.6‰ in February, and increases to 10.7‰ in May (Figure 5A). Subsequently, the $\delta^{15}N_{Nitrate}$ value decreases to −2.1‰ in August. The simulated ammonium in the surface layer is depleted in ^{15}N from May to September, and the minimum value is −1.1‰ in July (Figure 5B). The ammonium is enriched in ^{15}N from October to February, and reaches a maximum value of 6.0‰ in February. The

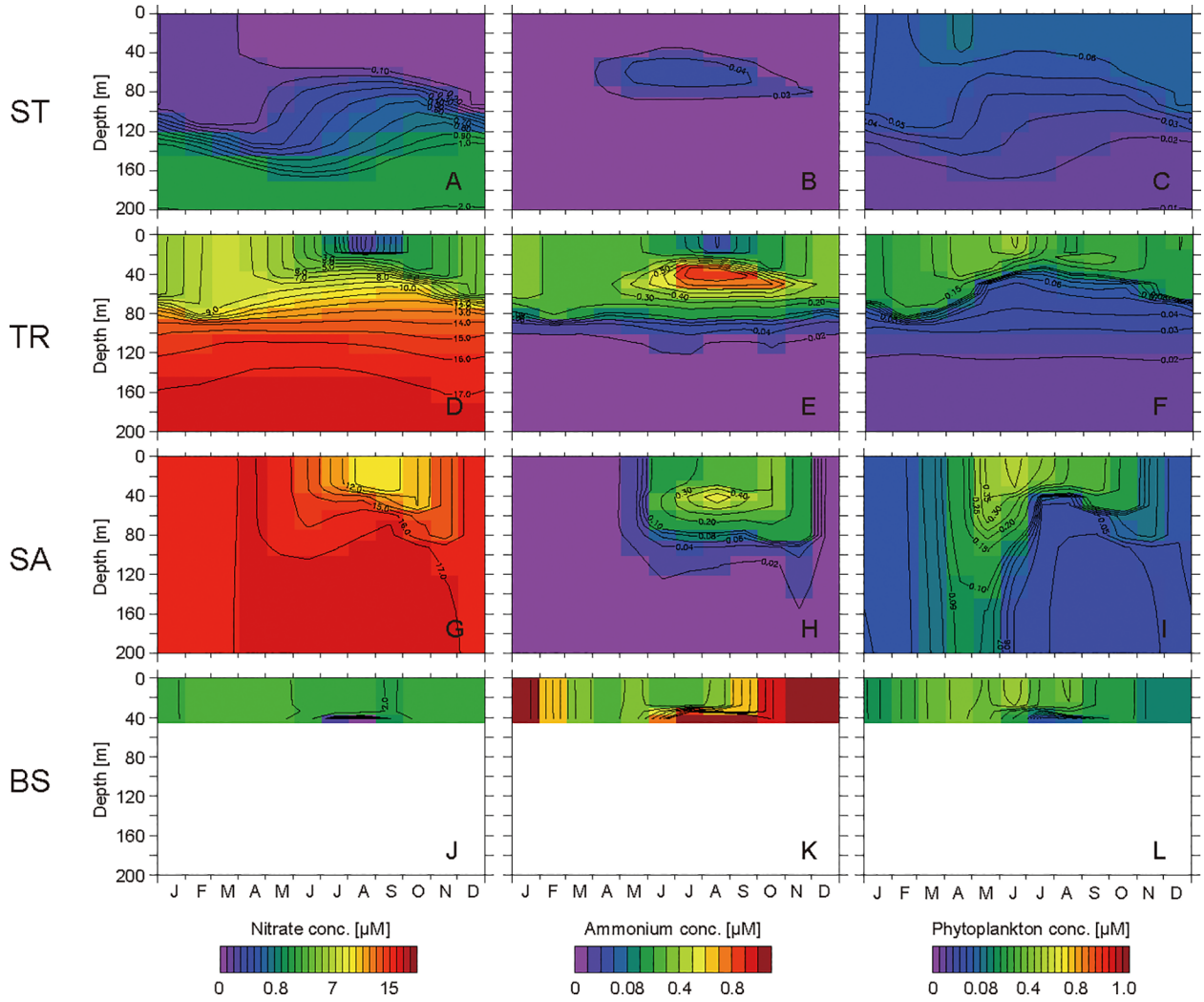

FIGURE 4
Seasonal cycles of simulated concentrations of nitrate, ammonium, and phytoplankton in the layers at 0–200 m at the western subtropical North Pacific site ST **(A–C)**, the Kuroshio–Oyashio transition zone site TR **(D–F)**, the western subarctic North Pacific site SA **(G–I)**, and the Bering Strait region site BS **(J–L)**.

simulated $\delta^{15}N_{Phytoplankton}$ value is 0.5‰ in the surface layer during a small bloom period in April, and is<0.0‰ from June to November (Figure 5C). The phytoplankton is enriched in ^{15}N and >2.0‰ in the layers at depths of 60–100 m from June to October.

At TR, the simulated $\delta^{15}N_{Nitrate}$ value in the surface layer is 6.2‰ in February (Figure 5D). The value increases to 17.0‰ in August, and then decreases gradually as the surface mixed layer deepens. The nitrate is slightly depleted in ^{15}N in the layers at depths of 40–140 m. The simulated ammonium in the surface layer is more depleted in ^{15}N than the nitrate from March to November, and the minimum value is 0.8‰ in May (Figure 5E). The ammonium is enriched in ^{15}N from September to February, and the maximum value is 7.8‰ in February. The simulated $\delta^{15}N_{Phytoplankton}$ value is 3.6‰ in the surface layer during the bloom period in June (Figure 5F). The phytoplankton in the surface layer has a minimum $\delta^{15}N$ value of 1.9‰ in May, and is subsequently enriched in ^{15}N to July and is depleted in ^{15}N to February as with the seasonal nitrate cycle. The phytoplankton is enriched in ^{15}N and >5.0‰ in the layers at depths of 30–90 m from July to January.

At SA, the simulated $\delta^{15}N_{Nitrate}$ value in the surface layer is 6.3‰ in February (Figure 5G), increases to 8.5‰ in August, and then decreases gradually as the surface mixed layer deepens. The seasonal variation in SA is similar to that in TR, although the amplitude is smaller. The simulated ammonium in the surface layer is more depleted in ^{15}N than nitrate from May to October, and the minimum value is −0.4‰ in July (Figure 5H). Subsequently, the ammonium is enriched in ^{15}N with a maximum value of 16.8‰ in December. The simulated $\delta^{15}N_{Phytoplankton}$ value is 1.4‰ in the surface layer during the bloom period in June and increases gradually to 4.2‰ in November (Figure 5I).

At BS, the simulated $\delta^{15}N_{Nitrate}$ value in the surface layer is 3.7‰ in January (Figure 5J). The value increases to 10.8‰ in August, and then decreases gradually as the surface mixed layer deepens. The simulated ammonium in the surface layer is more depleted in ^{15}N than nitrate from May to October, and the

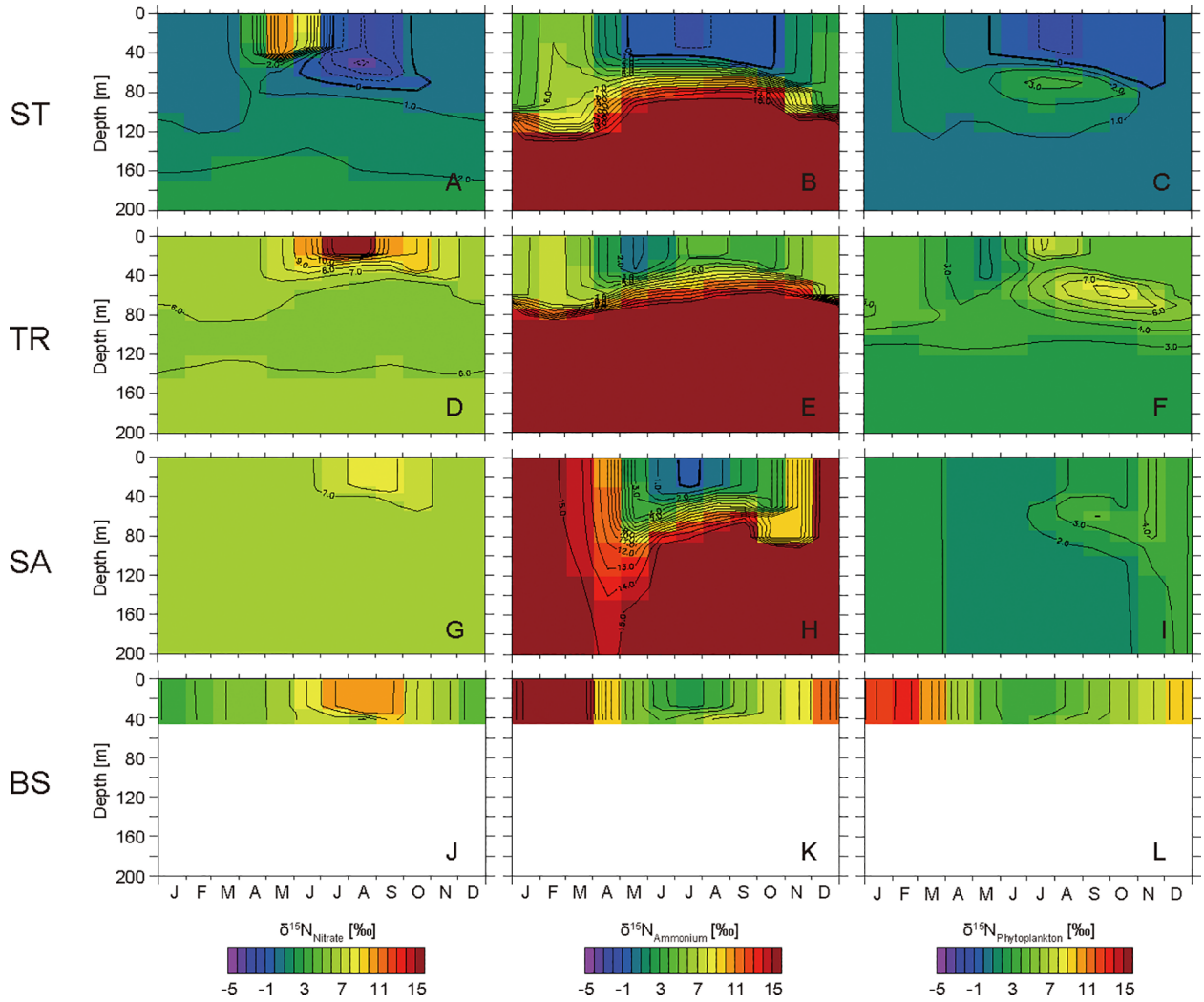

FIGURE 5
Seasonal cycles of simulated $\delta^{15}N$ values of nitrate, ammonium, and phytoplankton in the layers at 0–200 m at the western subtropical North Pacific site ST **(A–C)**, the Kuroshio–Oyashio transition zone site TR **(D–F)**, the western subarctic North Pacific site SA **(G–I)**, and the Bering Strait region site BS **(J–L)**.

minimum value is 2.4‰ in July (Figure 5K). Subsequently, the ammonium is enriched in ^{15}N with a maximum value of 17.9‰ in February. The simulated $\delta^{15}N_{Phytoplankton}$ values are 3.2‰ and 4.2‰ in the surface layer during bloom periods in June and August, respectively, and the value increases gradually to 13.6‰ in February (Figure 5L).

4 Discussion

4.1 Western subtropical North Pacific

The western subtropical North Pacific is characterized as an oligotrophic, low-productivity ocean (Figure 2). Active N_2 fixation occurs in the model due to nitrate depletion in the surface water throughout the year (Figure 6). The simulated annual mean $\delta^{15}N_{Phytoplankton}$ value in the euphotic layer at ST is 0.6‰, which is the lowest value among the selected sites. The diazotrophs take up N_2 gas, the $\delta^{15}N$ value of which is 0.0‰, and are remineralized to ammonium and nitrate. The phytoplankton takes up the ^{15}N-depleted ammonium and nitrate, and consequently is depleted in ^{15}N.

In winter, a small amount of nitrate is present in the surface water (Figure 4A). In early spring, the phytoplankton consumes the nitrate with an isotopic fractionation of 5‰ (Table 2). Therefore, the nitrate in the surface water is enriched in ^{15}N at the end of the small bloom (Figure 5A). In summer, the nitrate is completely consumed in the surface water, and the diazotrophs begin to take up N_2 actively (Figure 6B). N_2 fixation depletes ^{15}N in ammonium, nitrate, and phytoplankton in the surface water (Figures 5A–C).

Ammonium is produced by remineralization of PON, and is consumed by phytoplankton assimilation in the euphotic layer and by nitrification below the euphotic layer. As such, ammonium is accumulated at the bottom of the euphotic layer from spring to autumn (Figure 4B). The isotopic fractionation effect of ammonium assimilation by phytoplankton is as small as 0‰, and that of nitrification is as large as 14‰ (Table 2). As such, the ^{15}N enrichment of ammonium increases with depth (Figure 5B). The

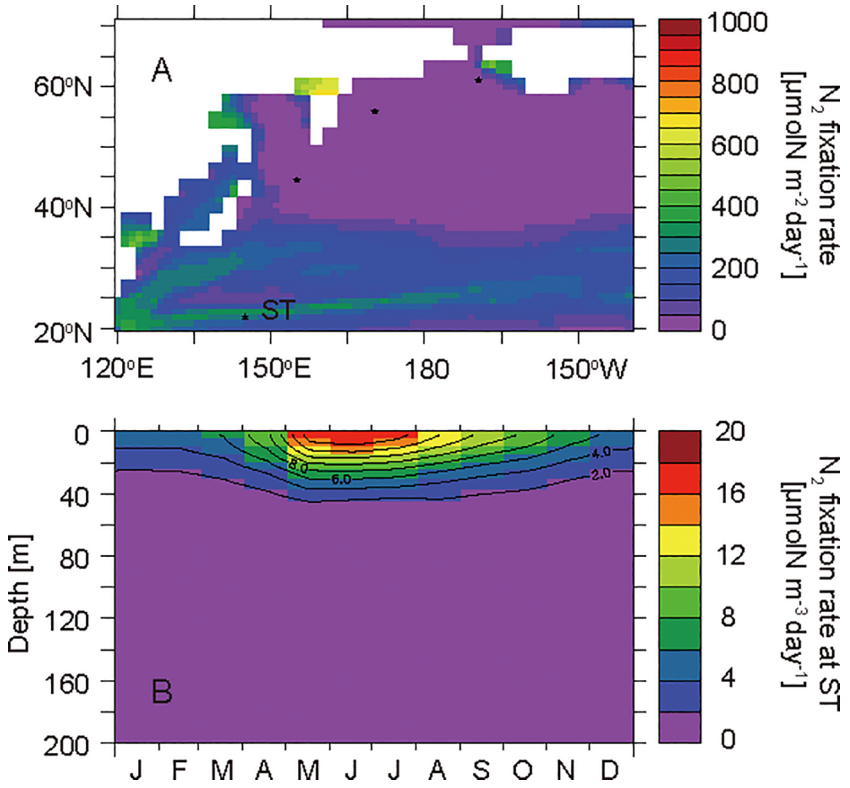

FIGURE 6
Horizontal distribution of annual mean N_2 fixation rates that were depth-integrated throughout the water column **(A)** and seasonal cycle of N_2 fixation rates in the layers at 0–200 m at the western subtropical North Pacific site ST **(B)**.

^{15}N-enriched ammonium in the subsurface water is supplied to the surface layer by the deepening of the mixed layer from autumn to winter.

4.2 Oyashio–Kuroshio transition zone

The Oyashio–Kuroshio transition zone in the western North Pacific is characterized as high-productivity ocean (Figure 2). The annual nitrate supply to the surface water is much higher than that at ST (Figures 4A, D), and the phytoplankton growth is limited only by nitrogen in the surface water (Figure 7A). Therefore, primary productivity is relatively high and phytoplankton exhausts nitrate in the surface water in summer. The simulated annual mean $\delta^{15}N_{Phytoplankton}$ value in the euphotic layer at TR is 3.9‰, which is a high value among the selected sites.

In winter, the nitrate in the surface water reaches its maximum concentration during the year due to winter convective mixing (Figure 4D). In spring, phytoplankton starts to consume the nitrate with an associated isotopic fractionation. Therefore,^{15}N enrichment of nitrate in the surface water proceeds toward summer (Figure 5D). In summer, nitrate is exhausted in the surface water and the maximum $\delta^{15}N_{Nitrate}$ value during the year is reached. Because phytoplankton actively assimilates nitrate, the seasonal variation in $\delta^{15}N_{Phytoplankton}$ is synchronized with that in $\delta^{15}N_{Nitrate}$ in the surface water (Figures 5D, F).

Ammonium accumulation is high in the subsurface water from spring to autumn due to active remineralization of PON (Figure 4E). The large isotopic fractionation of nitrification causes ^{15}N enrichment in ammonium and ^{15}N depletion in nitrate in the subsurface water (Figures 5D, E). The ^{15}N enrichment in phytoplankton in the subsurface water from summer to autumn is attributed to the phytoplankton assimilating ^{15}N-enriched ammonium (Figure 5F).

4.3 Western subarctic North Pacific

The western subarctic North Pacific is characterized as a high-nutrient low-chlorophyll ocean (Figure 2; e.g., Nishioka et al., 2020). Phytoplankton is affected by iron limitation and cannot assimilate all nitrate in the surface water in summer (Figure 7). The simulated annual mean $\delta^{15}N_{Phytoplankton}$ value in the euphotic layer at SA is 2.2‰, which is a low value among the selected sites. The low utilization of the surface nitrate pool by phytoplankton causes ^{15}N depletion in phytoplankton at SA, as suggested by Yoshikawa et al. (2018).

In winter, nitrate in the surface water reaches its maximum concentration during the year due to winter convective mixing (Figure 4G). In spring, phytoplankton starts to consume the nitrate with an associated isotopic fractionation, and thus the nitrate in the surface water is gradually enriched in ^{15}N toward summer

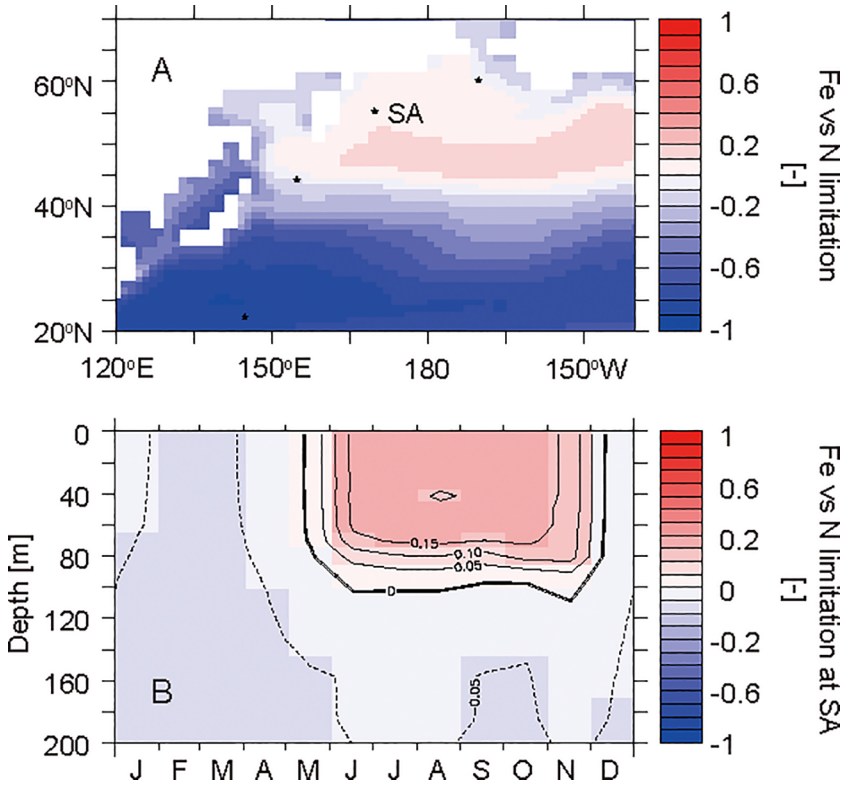

FIGURE 7
Horizontal distribution of the annual mean nutrient limitation (iron versus nitrogen) for phytoplankton in the surface layer **(A)** and the seasonal cycle in the layers at 0–200 m at the western subarctic North Pacific site SA **(B)**. The values were calculated from a nutrient-dependent term in the phytoplankton growth rate equation. Red shows the area where phytoplankton growth is limited by iron concentrations. Blue shows the area where phytoplankton growth is limited by nitrate and ammonium concentrations.

(Figure 5G). Because the nitrate assimilation by phytoplankton is limited by iron from May to December (Figure 7B), the minimum nitrate concentration and the maximum $\delta^{15}N_{Nitrate}$ value at SA are much higher and much lower than those at TR, respectively.

The ammonium is accumulated in the subsurface water from spring to autumn due to remineralization of PON (Figure 4H). As found at ST and TR, the ammonium is enriched in ^{15}N with depth at SA (Figure 5H). The ^{15}N-enriched ammonium in the subsurface water is supplied to the surface layer by the deepening of the mixed layer. From autumn to winter, the ammonium at SA is much more enriched in ^{15}N than that at TR. Because the phytoplankton assimilates the extremely ^{15}N-enriched ammonium (Figure 5I), the phytoplankton in the surface water from autumn to winter is the most enriched in ^{15}N during the year.

4.4 Bering Strait region

The Bering Strait region is characterized by a highly productive coastal ocean (Figure 2). The high sinking PON flux reaching the seafloor causes active benthic denitrification (Figure 8A). The depth of the ocean floor is only 41 m, and thus nitrification is inhibited by light in most of the water column (Figure 8B), and ammonium is not completely oxidized to nitrate throughout the year. The simulated annual mean $\delta^{15}N_{Phytoplankton}$ value in the euphotic layer at BS is 6.7‰, which is the highest value among the selected sites. The ^{15}N enrichment in phytoplankton is attributed to the uptake of highly-concentrated ^{15}N-enriched ammonium caused by partial nitrification and the removal of ^{15}N-depleted nitrate by benthic denitrification, as suggested by Granger et al. (2011).

In winter, nitrate in the surface water reaches its maximum concentration during the year (Figure 4J). In spring, phytoplankton starts to consume nitrate with an associated isotopic fractionation, and consequently the nitrate in the surface water is enriched in ^{15}N toward summer (Figure 5J). The $\delta^{15}N_{Nitrate}$ value in winter at BS is much lower than that at TR and SA due to incomplete nitrification with a large isotopic fractionation. The ^{15}N-depleted nitrate is removed from the benthic water by benthic denitrification after the bloom in June. The $\delta^{15}N_{Nitrate}$ value in the benthic water increases slightly with the decrease in nitrate concentration (Figures 4J and 5J) because the isotope fractionation during the benthic denitrification is small as 1‰ (Table 2).

Ammonium is not completely consumed by nitrification due to photo-inhibition throughout the water column, and thus ammonium accumulation is high in the benthic layer (Figures 4K and 8B). The ammonium is enriched in ^{15}N due to partial nitrification with a large isotopic fractionation. ^{15}N-enriched ammonium in the benthic water is supplied to the surface layer by the deepening of the mixed layer from autumn to winter and is gradually consumed by nitrification. As such, the $\delta^{15}N_{Ammonium}$ value in the surface water is high and varies drastically. As the phytoplankton takes up the ammonium throughout the year, the

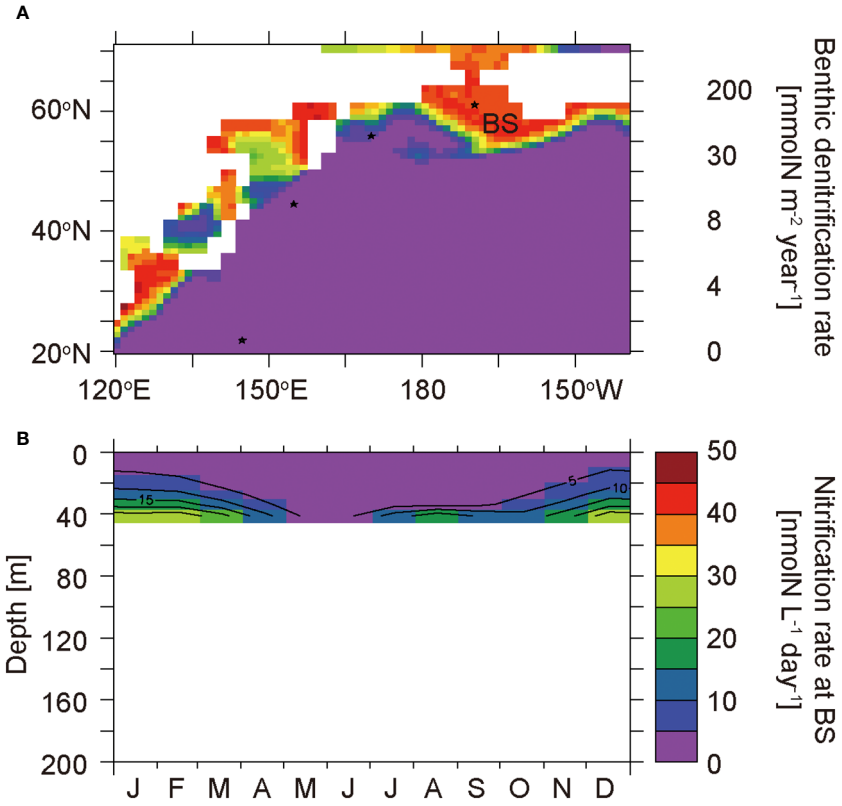

FIGURE 8
Horizontal distribution of benthic denitrification rates **(A)** and the seasonal cycle of nitrification rates in the layers at 0–41 m at the Bering Strait region site BS **(B)**.

$\delta^{15}N_{Phytoplankton}$ value at BS is high and is synchronized with the cycle of the $\delta^{15}N_{Ammonium}$ value (Figures 5K, L).

5 Summary

A seamless nitrogen isoscape of phytoplankton in the western North Pacific was created by using a marine nitrogen isotope model. The simulated annual average of $\delta^{15}N_{Phytoplankton}$ values in the euphotic layer ranged between −2.9‰ and 17.2‰ in the western North Pacific. Four distinctive sites were selected for discussion. At ST in the western subtropical North Pacific, the $\delta^{15}N_{Phytoplankton}$ value was as low as 0.6‰. The depletion in ^{15}N of phytoplankton was attributed to N_2 fixation. At TR in the Oyashio–Kuroshio transition zone, the $\delta^{15}N_{Phytoplankton}$ value was as high as 3.9‰. The ^{15}N enrichment of phytoplankton was attributed to the high utilization of the surface nitrate pool by phytoplankton. At SA in the western subarctic North Pacific, the $\delta^{15}N_{Phytoplankton}$ value was as low as 2.1‰. The depletion of ^{15}N in phytoplankton was attributed to the low utilization of the surface nitrate pool by phytoplankton due to iron limitation. At BS, the $\delta^{15}N_{Phytoplankton}$ value was as high as 6.7‰. The enrichment of ^{15}N in phytoplankton was attributed to partial nitrification with benthic denitrification.

The $\delta^{15}N_{Phytoplankton}$ value showed a characteristic seasonal variation at each site. At ST, the $\delta^{15}N_{Phytoplankton}$ value varied from −1.1‰ to 1.3‰. The nitrate and ammonium were exhausted and N_2 fixation occurred throughout the year. Because the N_2 and recycled ammonium supported most of the production, the seasonal variation in $\delta^{15}N_{Phytoplankton}$ at ST was as small as 2.4‰. At TR, the $\delta^{15}N_{Phytoplankton}$ values varied from 1.9‰ to 7.1‰. Convective mixing supplied nitrate from the subsurface to the surface in winter. Because phytoplankton consumes nitrate almost completely with an associated isotopic fractionation, nitrate was enriched greatly in ^{15}N from 6.2‰ to 17.0‰, and subsequently phytoplankton was also enriched greatly in ^{15}N. The high utilization of nitrate by phytoplankton caused the large seasonal variation in $\delta^{15}N_{Phytoplankton}$ values of 5.2‰. At SA, the $\delta^{15}N_{Phytoplankton}$ values varied from 1.3‰ and 4.2‰. The phytoplankton was affected by iron limitation and could not consume nitrate completely. The low utilization of nitrate by phytoplankton causes the relatively small seasonal variation in $\delta^{15}N_{Phytoplankton}$ values of 2.9‰. At BS, the $\delta^{15}N_{Phytoplankton}$ values varied from 3.2‰ and 13.6‰. The ammonium concentration was extremely high throughout the year due to partial nitrification. As nitrification proceeded gradually from autumn to winter with a large isotopic fractionation, ammonium was greatly enriched in ^{15}N from 2.5‰ to 17.9‰. Because phytoplankton assimilates the ammonium, the seasonal variation in $\delta^{15}N_{Phytoplankton}$ values at BS was as large as 10.4‰.

The annual mean $\delta^{15}N_{Phytoplankton}$ value had sufficient spatial variations (e.g., 0.6‰ at ST, 3.9‰ at TR, 2.1‰ at SA, and 6.7‰ at BS) for iso-logging studies in the western North Pacific compared with the analytical errors of the $\delta^{15}N_{Base}$ values of fish ($1\sigma < \pm$ 0.8‰) (Matsubayashi et al., 2017; Matsubayashi et al., 2020; Harada et al.,

2022). The seasonal variability of $\delta^{15}N_{Phytoplankton}$ reached 5.2‰ at TR and 10.4‰ at BS, which were greater than the spatial variability in the western North Pacific. To trace the movement of fish whose habitat is expected to include those areas, the seasonal variations of the nitrogen isoscape should be considered carefully.

Both $\delta^{15}N_{Base}$ values of fish and a nitrogen isoscape of phytoplankton are needed for iso-logging studies. The estimation of $\delta^{15}N_{Base}$ values requires the $\delta^{15}N$ measurement of amino acids to correct for ^{15}N-enrichment of ~3‰ per trophic position of the $\delta^{15}N$ values of bulk nitrogen of fish (Matsubayashi et al., 2017; Matsubayashi et al., 2020; Harada et al., 2022). However, because the $\delta^{15}N$ measurement of amino acids still takes much time and effort, there have been a few previous studies of the $\delta^{15}N$ values of amino acids. Nitrogen isoscapes of diet (zooplankton or small fish) using a nitrogen isotope model, including higher-trophic-level organisms, will advance iso-logging studies.

Data availability statement

The raw data supporting the conclusions of this article will be made available by the authors, without undue reservation.

Author contributions

CY: Conceptualization, Data curation, Formal Analysis, Funding acquisition, Methodology, Project administration, Software, Validation, Visualization, Writing – original draft, Writing – review & editing. MS: Conceptualization, Methodology, Software, Writing – review & editing. AY: Conceptualization, Methodology, Software, Writing – review & editing. AO: Conceptualization, Methodology, Software, Writing – review & editing. NO: Conceptualization, Funding acquisition, Project administration, Supervision, Writing – review & editing.

Funding

The author(s) declare financial support was received for the research, authorship, and/or publication of this article. We acknowledge support from JSPS KAKENHI Grants 19H04247, 19KK0293, 19K22917 20KK0165, and 21H03579. MS acknowledges support from JSPS KAKENHI Grants 18H04129 and 19H04246.

Acknowledgments

We thank D.M. Sigman, P.A. Rafter, an reviewer, and the editor for their valuable comments, and D. Marconi for suggestions about compiling the $D_{15}N_{Nitrate}$ data. The simulations with a nitrogen isotope model were performed using the Earth Simulator (ES4) at JAMSTEC. This study is partially supported by the Cooperative Research Activities of Collaborative Use of Computing Facility of the Atmosphere and Ocean Research Institute, the University of Tokyo. The analysis and graphics in this paper employed the Ferret program of NOAA's Pacific Marine Environmental Laboratory.

Conflict of interest

The authors declare that the research was conducted in the absence of any commercial or financial relationships that could be construed as a potential conflict of interest.

Publisher's note

All claims expressed in this article are solely those of the authors and do not necessarily represent those of their affiliated organizations, or those of the publisher, the editors and the reviewers. Any product that may be evaluated in this article, or claim that may be made by its manufacturer, is not guaranteed or endorsed by the publisher.

Supplementary material

The Supplementary Material for this article can be found online at: https://www.frontiersin.org/articles/10.3389/fmars.2024.1294608/full#supplementary-material

References

Bianchi, D., Dunne, J. P., Sarmiento, J. L., and Galbraith, E. D. (2012). Data-based estimates of suboxia, denitrification, and N_2O production in the ocean and their sensitivities to dissolved O_2. *Global Biogeochem. Cycles* 26, GB2009. doi: 10.1029/2011GB004209

Bohlen, L., Dale, A. W., and Wallmann, K. (2012). Simple transfer functions for calculating benthic fixed nitrogen losses and C:N:P regeneration ratios in global biogeochemical models. *Global Biogeochem. Cycles* 26, GB3029. doi: 10.1029/2011GB004198

Coles, V. J., and Hood, R. R. (2007). Modeling the impact of iron and phosphorus limitations on nitrogen fixation in the Atlantic Ocean. *Biogeoscienced* 4, 455–497. doi: 10.5194/bg-4-455-2007

Coles, V. J., Hood, R. R., Pascual, M., and Capone, D. G. (2004). Modeling the effects of Trichodesmium and nitrogen fixation in the Atlantic Ocean. *J. Geophys. Res.* 109, C06007. doi: 10.01029/02002JC001754

DeVries, T., Deutsch, C., Rafter, P. A., and Primeau, F. (2013). Marine denitrification rates determined from a global 3-D inverse model. *Biogeosciences* 10, 2481–2496. doi: 10.5194/bg-10-2481-2013

FAO (2022). "The state of world fisheries and aquaculture 2022," in *Towards Blue Transformation* (Rome, Italy: Food and Agriculture Organization of the United Nations (FAO)). doi: 10.4060/cc0461en

Fripiat, F., Marconi, D., Rafter, P. A., Sigman, D. M., Altabet, M. A., Bourbonnais, A., et al. (2021). Compilation of nitrate δ^{15}N in the ocean. *PANGAEA*. doi: 10.1594/PANGAEA.936484

Garcia, H. E., Weathers, K., Paver, C. R., Smolyar, I., Boyer, T. P., Locarnini, R. A., et al. (2019). World Ocean Atlas 2018, Volume 4: Dissolved Inorganic Nutrients (phosphate, nitrate and nitrate+nitrite, silicate). *A. Mishonov Tech. Ed.; NOAA Atlas NESDIS* 84, 35.

Granger, J., Prokopenko, M. G., Sigman, D. M., Mordy, C. W., Morse, Z. M., Morales, L. V., et al. (2011). Coupled nitrification-denitrification in sediment of the eastern Bering Sea shelf leads to ^{15}N enrichment of fixed N in shelf waters. *J. Geophys. Res.* 116, C11006. doi: 10.1029/2010JC006751

Granger, J., Sigman, D. M., Lehmann, M. F., and Tortell, P. D. (2008). Nitrogen and oxygen isotope fractionation during dissimilatory nitrate reduction by denitrifying bacteria. *Limnol. Oceanogr.* 53 (6), 2533–2545. doi: 10.4319/lo.2008.53.6.2533

Granger, J., Sigman, D. M., Rohde, M. M., Maldonado, M. T., and Tortell, P. D. (2010). N and O isotope effects during nitrate assimilation by unicellular prokaryotic and eukaryotic plankton cultures. *Geochim. Cosmochim. Acta* 74, 1030–1040. doi: 10.1016/j.gca.2009.10.044

Hajima, T., Watanabe, M., Yamamoto, A., Tatebe, H., Noguchi, M. A., Abe, M., et al. (2020). Development of the MIROC-ES2L Earth system model and the evaluation of biogeochemical processes and feedbacks. *Geosci. Model. Dev.* 13, 2197–2244. doi: 10.5194/gmd-13-2197-2020

Hanselman, D. H., Heifetz, J., Echave, K. B., and Dressel, S. C. (2015). Move it or lose it: movement and mortality of sablefish tagged in Alaska. *Can. J. Fisheries Aquat. Sci.* 72, 238–251. doi: 10.1139/cjfas-2014-0251

Harada, Y., Ito, S., Ogawa, N. O., Yoshikawa, C., Ishikawa, N. F., Yoneda, M., et al. (2022). Compound-specific nitrogen isotope analysis of amino acids in eye lenses as a new tool to reconstruct the geographic and trophic histories of fish. *Front. Mar. Sci.* 8. doi: 10.3389/fmars.2021.796532

Hays, G. C., Ferreira, L. C., Sequeira, A. M., Meekan, M. G., Duarte, C. M., Bailey, H., et al. (2016). Key questions in marine megafauna movement ecology. *Trends Ecol. Evol.* 31, 463–475. doi: 10.1016/j.tree.2016.02.015

Hood, R. R., Bates, N. R., Capone, D. G., and Olson, D. B. (2001). Modeling the effect of nitrogen fixation on carbon and nitrogen fluxes at BATS. *Deep-Sea Res. II* 48, 1609–1648. doi: 10.1016/S0967-0645(00)00160-0

Hood, R. R., Coles, V. J., and Capone, D. G. (2004). Modeling the distribution of Trichodesmium and nitrogen fixation in the Atlantic Ocean. *J. Geophys. Res.* 109, C06006. doi: 10.1029/2002JC001753

Letscher, R. T., Hansell, D. A., Carlson, C. A., Lumpkin, R., and Knapp, A. N. (2013). Dissolved organic nitrogen in the global surface ocean: Distribution and fate, Global Biogeochem. *Cycles* 27, 141–153. doi: 10.1029/2012GB004449

Liu, K.-K., Kao, S.-J., Chiang, K.-P., Gong, G.-C., Chang, J., Cheng, J.-S., et al. (2013). Concentration dependent nitrogen isotope fractionation during ammonium uptake by phytoplankton under an algal bloom condition in the Danshuei estuary, northern Taiwan. *Mar. Chem.* 157, 242–252. doi: 10.1016/j.marchem.2013.10.005

Lowerre-Barbieri, S. K., Kays, R., Thorson, J. T., and Wikelski, M. (2019). The ocean's movescape: fisheries management in the bio-logging decade, (2018–2028). *ICES J. Mar. Sci.* 76, 477–488. doi: 10.1093/icesjms/fsy211

Matsubayashi, J., Kimura, K., Ohkouchi, N., Ogawa, N. O., Ishikawa, N. F., Chikaraishi, Y., et al. (2022). Using geostatistical analysis for simultaneous estimation of isoscapes and ontogenetic shifts in isotope ratios of highly migratory marine fish. *Front. Mar. Sci.* 9. doi: 10.3389/fmars.2022.1049056

Matsubayashi, J., Osada, Y., Tadokoro, K., Abe, Y., Yamaguchi, A., Shirai, K., et al. (2020). Tracking long-distance migration of marine fishes using compound-specific stable isotope analysis of amino acids. *Ecol. Lett.* 23, 881–890. doi: 10.1111/ele.13496

Matsubayashi, J., Saitoh, Y., Osada, Y., Uehara, Y., Habu, J., Sasaki, T., et al. (2017). Incremental analysis of vertebral centra can reconstruct the stable isotope chronology of teleost fishes. *Methods Ecol. Evol.* 8, 1755–1763. doi: 10.1111/2041-210X.12834

McMahon, K. W., Hamady, L., and Thorrold, S. R. (2013). A review of ecogeochemistry approaches to estimating movements of marine animals. *Limnol. Oceanogr.* 58, 697–714. doi: 10.4319/lo.2013.58.2.0697

Minagawa, M., and Wada, E. (1984). Stepwise enrichment of 15N along food chains: Further evidence and the relation between d15N and animal age. *Geochim. Cosmochim. Acta* 48, 1135–1140. doi: 10.1016/0016-7037(84)90204-7

Minagawa, M., and Wada, E. (1986). Nitrogen isotope ratio of red tide organisms in the East China Sea: A characterization of biological nitrogen fixation. *Mar. Chem.* 19, 245–259. doi: 10.1016/0304-4203(86)90026-5

Montoya, J. P., and McCarthy, J. J. (1995). Isotopic fractionation during nitrate uptake by phytoplankton grown in continuous culture. *J. Plankton Res.* 17, 439–464. doi: 10.1093/plankt/17.3.439

Nishioka, J., Obata, H., Ogawa, H., Ono, K., Yamashita, Y., Lee, K., et al. (2020). Subpolar marginal seas fuel the North Pacific through the intermediate water at the termination of the global ocean circulation. *Proc. Natl. Acad. Sci.* 117 (23), 202000658–202000658. doi: 10.1073/pnas.2000658117

Oka, A., Kato, S., and Hasumi, H. (2008). Evaluating effect of ballast mineral on deep-ocean nutrient concentration by using an ocean general circulation model. Global Biogeochem. *Cycles* 22, GB3004. doi: 10.1029/2007GB003067

O'Reilly, J. E., Maritorena, S., Mitchell, B. G., Siegal, D. A., Carder, K. L., Garver, S. A., et al. (1998). Ocean color chlorophyll algorithms for SeaWiFS. *J. Geophys. Res.* 103, 24937–24953. doi: 10.1029/98JC02160

Rafter, P., Bagnell, A., DeVries, T., and Marconi, D. (2019). Compiled dataset consisting of published and unpublished global nitrate d15N measurements from from 1975-2018. *Biol. Chem. Oceanogr. Data Manage. Office*. doi: 10.1575/1912/bco-dmo.768627.1

Schmittner, A., Oschlies, A., Matthews, H. D., and Galbraith, E. D. (2008). Future changes in climate, ocean circulation, ecosystems and biogeochemical cycling simulated for a business-as-usual CO2 emission scenario until year 4000 AD. *Global Biogeochem. Cycles* 22, GB1013. doi: 10.1029/2007GB002953

Shigemitsu, M., Gruber, N., Oka, A., and Yamanaka, Y. (2016). Potential use of the N_2/Ar ratio as a constraint on the oceanic fixed nitrogen loss. *Global Biogeochem. Cycles* 30, 576–594. doi: 10.1002/2015GB005297

Shigemitsu, M., Yamamoto, A., Oka, A., and Yamanaka, Y. (2017). One possible uncertainty in CMIP5 projections of low-oxygen water volume in the Eastern Tropical Pacific. *Global Biogeochem. Cycles* 31, 804–820. doi: 10.1002/2016GB005447

Somes, C., Oschlies, J. A., and Schmittner, A. (2013). Isotopic constraints on the pre-industrial oceanic nitrogen budget. *Biogeosciences* 10, 5889–5910. doi: 10.5194/bg-10-5889-2013

Somes, C. J., Schmittner, A., Galbraith, E. D., Lehmann, M. F., Altabet, M. A., Montoya, J. P., et al. (2010). Simulating the global distribution of nitrogen isotopes in the ocean. Global Biogeochem. *Cycles* 24, GB4019. doi: 10.1029/2009GB003767

Somes, C. J., Schmittner, A., Muglia, J., and Oschlies, A. (2017). A three-dimensional model of the marine nitrogen cycle during the last glacial maximum constrained by sedimentary isotopes. *Front. Mar. Sci.* 4. doi: 10.3389/fmars.2017.00108

Tesdal, J. E., Galbraith, E. D., and Kienast, M. (2013). Nitrogen isotopes in bulk marine sediment: linking seafloor observations with subseafloor records. *Biogeosciences* 10, 101–118. doi: 10.5194/bg-10-101-2013

Thorson, J. T., Jannot, J., Somers, K., and Punt, A. (2016). Using spatio-temporal models of population growth and movement to monitor overlap between human impacts and fish populations. *J. Appl. Ecol.* 54, 577–587. doi: 10.1111/1365-2664.12664

Tzadik, O. E., Curtis, J. S., Granneman, J. E., Kurth, B. N., Pusack, T. J., Wallace, A. A., et al. (2017). Chemical archives in fishes beyond otoliths: a review on the use of other body parts as chronological recorders of microchemical constituents for expanding interpretations of environmental, ecological, and life-history changes. *Limnol. Oceanogr.: Methods* 15, 238–263. doi: 10.1002/lom3.10153

Vecchio, J. L., and Peebles, E. B. (2020). Spawning origins and ontogenetic movements for demersal fishes: An approach using eye-lens stable isotopes. *Estuar. Coast. Shelf. Sci.* 246, 107047. doi: 10.1016/j.ecss.2020.107047

Wada, E., and Hattori, A. (1978). Nitrogen isotope effects in the assimilation of inorganic nitrogenous compounds by marine diatoms. *Geomicrobiol. J.* 1, 85–101. doi: 10.1080/01490457809377725

Watanabe, S., Hajima, T., Sudo, K., Nagashima, T., Takemura, T., Okajima, H., et al. (2011). MIROC-ESM 2010: Model description and basic results of CMIP5-20c3m experiments, Geosci. *Model. Dev.* 4, 845–872. doi: 10.5194/gmd-4-845-2011

Yamamoto, A., Abe-Ouchi, A., Ohgaito, R., Ito, A., and Oka, A. (2019). Glacial CO_2 decrease and deep-water deoxygenation by iron fertilization from glaciogenic dust. *Climate Past* 15 (3), 981–996. doi: 10.5194/cp-15-981-2019

Yoshikawa, C., Abe, H., Aita, M. N., Breider, F., Kuzunuki, K., Toyoda, S., et al. (2016). Insight into nitrous oxide production processes in the western North Pacific based on a marine ecosystem isotopomer model. *J. Oceanogr.* 72 (3), 491–508. doi: 10.1007/s10872-015-0308-2

Yoshikawa, C., Coles, V. J., Hood, R. R., Capone, D. G., and Yoshida, N. (2013). Modeling how surface nitrogen fixation influences subsurface nutrient patterns in the North Atlantic. *J. Geophys. Res. Oceans* 118, 2520–2534. doi: 10.1002/jgrc.20165

Yoshikawa, C., Makabe, A., Matsui, Y., Nunoura, T., and Ohkouchi, N. (2018). Nitrate isotope distribution in the subarctic and subtropical North Pacific. *Geochem. Geophys. Geosystems* 19, 2212–2224. doi: 10.1029/2018GC007528

Yoshikawa, C., Ogawa, N. O., Chikaraishi, Y., Makabe, A., Matsui, Y., Sasai, Y., et al. (2022). Nitrogen isotopes of sinking particles reveal the seasonal transition of the nitrogen source for phytoplankton. *Geophys. Res. Lett.* 49, e2022GL098670. doi: 10.1029/2022GL098670

Yoshikawa, C., Yamanaka, Y., and Nakatsuka, T. (2005). An ecosystem model including nitrogen isotopes: Perspectives on a study of the marine nitrogen cycle. *J. Oceanogr.* 61 (5), 921–942. doi: 10.1007/s10872-006-0010-5